ASCE

Shake-Table Test of a Seismically Resilient 10-Story Mass Timber Building with Supplemental Uplift Friction Dampers

Daniel M. Dowden, M.ASCE[1]; Arman Tatar, S.M.ASCE[2]; Jeffrey W. Berman, A.M.ASCE[3]; and Shiling Pei, F.ASCE[4]

Abstract: Post-tensioned rocking mass timber walls (PT-RMTWs) have been established as a seismically resilient seismic force-resisting system for mass timber buildings with high potential. The literature is rich in experimental studies that show that mass timber walls exhibit rocking wall behavior but require supplemental damping systems to dissipate energy during an earthquake. In this experimental study, the dynamic seismic response of a recently introduced low-damage uplift friction damper (UFD) for PT-RMTWs is validated. Experimental tests were conducted as a separate payload project using the Natural Hazards Engineering Research Infrastructure (NHERI) TallWood large-scale 10-story mass timber building shake-table test specimen. Tests were conducted at the NHERI Large High Performance Outdoor Shake Table at the University of California, San Diego. This paper reports the results of this experimental test program with the UFDs along with some limited comparisons to numerical results. First, the global response of the test building is presented. Second, local and global behavior of the UFDs installed on the test building is highlighted. Third, a comparison of building response with and without the UFDs of the test building is presented. Lastly, some limited comparisons are made with the experimental results with those predicted obtained from a nonlinear response history analysis of a numerical model of the test building. The reported experimental results show that the UFDs enhanced the seismic response of the test building quantified by increasing the lateral strength, reducing the peak interstory drifts, and adding energy dissipation. **DOI: 10.1061/JSENDH.STENG-13788.**

Author keywords: Cross-laminated timber (CLT); Mass timber; Friction; Damper; Seismic; Resilience.

Introduction

Cross-laminated timber (CLT) has recently emerged as an innovative construction material for mass timber building construction within the United States (US) and has also paved the way for other more recent mass timber panel products (e.g., mass plywood panel, dowel laminated timber, etc.). Benefits of these structural products include rapid construction, high strength-to-weight ratio, fire resistance, ecosustainability, and low embodied carbon footprint (Green and Karsh 2012; Pei et al. 2016). Of significance, CLT has provided a pathway for the potential of tall (i.e., 8–18 stories) mass timber building alternatives that were not possible before in the US, where traditional light framed timber structures are typically restricted to five to six stories maximum (IBC 2015). In the US, tall mass timber buildings that use prescriptive design methods currently require a hybrid solution, i.e., using mass timber panels to support gravity loads, whereby lateral seismic/wind forces are resisted by conventional lateral force resisting systems (LFRSs) constructed of steel and/or concrete. Recently, CLT shear wall seismic performance factors have been established for use as the first mass timber SFRSs to be adopted in the US building codes (van de Lindt et al. 2020). Although a significant achievement, the lateral system is still limited to buildings with six stories or fewer.

Challenges exist that limit the use of mass timber based seismic force-resisting systems (SFRSs) for tall buildings. These challenges include lack of appropriate mass timber specific seismic energy dissipation devices/connections and knowledge gaps in seismic performance of tall mass timber building systems subjected to dynamic earthquake loadings. Post-tensioned rocking mass timber walls (PT-RMTWs) have emerged as SFRSs that show promise in advancing mass timber technologies. Recent research has shown that PT-RMTWs are feasible and have the benefit of being inherently seismically resilient compared with conventional code-based prescriptive SFRSs. Specifically, PT-RMTWs can provide building self-centering and concentrate inelastic energy dissipation (damage) to replaceable elements (i.e., structural fuses). Unlike seismically resilient SFRSs, the inelastic energy dissipation elements of conventional SFRSs are coupled with the gravity frame system, leading to irreparable structural damage, and large residual building drifts remain after a moderate to large earthquake, leaving the building vulnerable to possible collapse. Consequently, buildings with conventional SFRSs would likely face demolition after a large seismic event. The 2010–2011 Christchurch earthquakes and the rebuilding of Christchurch (where buildings were designed with modern seismic codes, construction material, and practices) has highlighted this issue (Bruneau and MacRae 2017).

Scaled wall subassemblage and three dimensional (3D) large-scale building experiments have validated that slender CLT shear walls remain essentially elastic and exhibit a rocking dominated behavior under lateral loadings (Ceccotti et al. 2013; Gavric et al. 2015; Hristovski et al. 2013; Popovski and Gavric 2016;

[1]Assistant Professor, Dept. of Civil, Environmental, and Geospatial Engineering, Michigan Technological Univ., Houghton, MI 49931 (corresponding author). ORCID: https://orcid.org/0000-0002-5244-6093. Email: dmdowden@mtu.edu

[2]Graduate Research Assistant, Dept. of Civil, Environmental, and Geospatial Engineering, Michigan Technological Univ., Houghton, MI 49931. ORCID: https://orcid.org/0000-0001-5729-9451. Email: atatar@mtu.edu

[3]Professor, Dept. of Civil and Environmental Engineering, Univ. of Washington, Seattle, WA 98195. Email: jwberman@uw.edu

[4]Associate Professor, Dept. of Civil and Environmental Engineering, Colorado School of Mines, Golden, CO 80401. Email: spei@mines.edu

Note. This manuscript was submitted on February 20, 2024; approved on July 15, 2024; published online on November 6, 2024. Discussion period open until April 6, 2025; separate discussions must be submitted for individual papers. This paper is part of the ***Journal of Structural Engineering***, © ASCE, ISSN 0733-9445.

Popovski et al. 2010; van de Lindt et al. 2019). Consequently, the use of conventional metal shear connectors and hold-down uplift anchors intended for light-framed timber construction are not well suited for mass timber SFRSs. Particularly, hold-down uplift anchors are highly vulnerable to rapid deterioration due to the uplift rocking motion of CLT panels (Izzi et al. 2018; Liu and Lam 2019; Popovski et al. 2010; Pozza et al. 2018). Furthermore, leveraging on the natural rocking behavior observed from CLT shear wall tests, researchers have more recently investigated PT-RMTWs (Akbas et al. 2017; Ganey et al. 2017; Sarti et al. 2013; Smith et al. 2007). As noted earlier, this next evolution in mass timber SFRSs has led to seismically resilient mass timber buildings, where performance objectives consider rapid structural repairability and occupancy after a significant seismic event. In these studies, adopting principles used by the PRESS program (Priestley et al. 1999), vertically oriented steel post-tensioning (PT) elements are provided along the full height of the mass timber wall panels. Through near rigid rocking wall motion, the elastic elongation of the PT elements provides a building self-centering response. These past studies have highlighted that energy dissipating elements are needed that integrate holistically with the natural kinematics of these SFRSs.

An approach for providing seismic energy dissipation for PT-RMTWs has been the use of hysteretic metallic yielding structural fuses located at the foundation base of the wall (Kramer et al. 2016; Sarti et al. 2016; Smith et al. 2007). These elements adopt similar principles as buckling-restrained-braces (BRB) used in conventional braced-frame SFRSs (ASCE 2017), which provide energy dissipation in both uniaxial tension and compression. However, adaptation for use with PT-RMTWs require significant scale-down of these mini-BRBs (Maurya et al. 2016; Sarti et al. 2013), limiting the energy dissipation and making them sensitive to tensile rupture due to the large strain demands upon wall rocking uplift. Accordingly, mini-BRB type structural fuses may not be appropriate for tall mass timber buildings where large seismic force and drift demands are expected. An alternative approach has been the use of interpanel shear connectors or coupled-walls (Akbas et al. 2017; Ganey et al. 2017; Iqbal et al. 2015). The benefit includes a greater level of energy dissipation capability along with uniform distribution of energy dissipation along the building height, which is well suited for tall buildings. Furthermore, energy dissipation is provided through flexure versus uniaxial tension/compression, significantly reducing the potential of tensile strain rupture (Kelly et al. 1972). This approach was used by the NHERI project team for the PT-RMTWs (Blomgren et al. 2019; Pei et al. 2019; van de Lindt et al. 2019) and adopted for their NHERI TallWood 10-story building shake-table tests. However, as with all yielding elements, interpanel shear connectors are susceptible to strength and stiffness degradation and may need to be replaced post-event. Other forms of hysteretic metallic yielding dampers have been proposed (Polastri et al. 2018; Trutalli et al. 2019), but most are proprietary in nature and inherently rely on inelastic damage. To overcome some of these limitations of hysteretic metallic yielding dampers in PT-RMTWs, others have investigated friction-based dampers that provide stable energy dissipation where repair is not expected post-event (Hashemi et al. 2018; Loo et al. 2016).

To advance knowledge of tall mass timber building systems toward practical implementation, as a final proof-of-concept of the NHERI TallWood project, the TallWood project team (Pei et al., forthcoming) designed a large-scale 10-story mass timber building for testing at the NHERI outdoor shake table at the University of California, San Diego (UCSD). This test is the first large-scale, tall mass timber building shake-table test with PT-RMTW rocking walls. These tests were completed in June 2023. This benchmark test program has validated the realization of tall mass timber buildings with seismically resilient mass timber-based SFRSs. Based on the culmination of research established from the NHERI TallWood project leading up to these large-scale shake-table tests (Furley et al. 2021; Ganey et al. 2017; Pei et al. 2019, 2021; Wichman et al. 2022a), the mass timber rocking wall SFRSs were detailed with U-shaped flexural steel plate (UFP) energy dissipators (Kelly et al. 1972). Although the use of these dampers showed excellent performance, hysteretic yielding dampers have limitations including stiffness and strength degradation, potential fracture due to accumulated plastic deformation, and no potential for self-centering capacity. Furthermore, although these hysteretic yielding dampers were shown to isolate controlled damage to the sacrificial elements detailed to be replaced, practical challenges could remain in replacing these elements post-seismic event. To overcome some of these limitations, this payload research project investigated a low-damage uplift friction damper (UFD) for mass timber rocking walls that provides stable energy dissipation and enhanced self-centering capabilities and eliminates the need for repair/replacement of these devices post-seismic event. For this purpose, after the NHERI TallWood team completed their tests, UFDs were installed, and additional earthquake tests were conducted. This paper presents the experimental results and findings of these additional shake-table tests to validate the performance of the proposed UFDs subjected to real simulated earthquakes on a test building with realistic boundary conditions.

Background

Uplift Friction Damper

The proposed uplift friction dampers (UFDs) are expected to provide stable energy dissipation and some self-centering capabilities while using friction plates that are easily replaceable after a design level seismic event if needed. General details of the proposed friction damper for a PT-RMTW rocking wall is schematically shown in Fig. 1 (note that the schematic shown is not the exact configuration used in this testing program). In that detail, energy dissipation is provided through abrasive friction from the relative sliding between two angled steel wedges. Here, one wedge is attached directly to the sides of the PT-RMTW (referenced as the "vertical" wedge). A second wedge is attached to a tension rod bolted to the foundation that resists the uplift wall forces (referenced as the "horizontal" wedge). Note that the reference of the vertical and horizontal wedge refers to the motion of the wedges when the wall uplifts at the UFD locations due to wall rocking. The vertical wedge attached to the wall moves primarily in the vertical direction with the wall, and the horizontal wedge anchored to the uplift tension rod moves primarily in the horizontal direction out-of-plane from the wall. The two wedges are clamped together with high strength thru-rods, where the wedge attached to the PT-RMTW is detailed with vertically slotted holes to accommodate the relative movement between the two wedges. The anchor tension rods are detailed with pinned connections at each end to allow unrestrained rotation at these connection points and relative movement of the steel friction wedges. Connections of the damper to the PT-RMTW are provided through fully threaded self-tapping screws positioned at 45° about the surface of the wall panel. Out of plane stability for the PT-RMTW is provided by shear keys. Furthermore, shear keys are provided in the in-plane direction to transfer the base shear to the foundation at the toes of the wall. Post-tensioned elements are provided at the mid length of the wall to provide wall self-centering. In general, the kinematics of the UFDs is independent of the wall

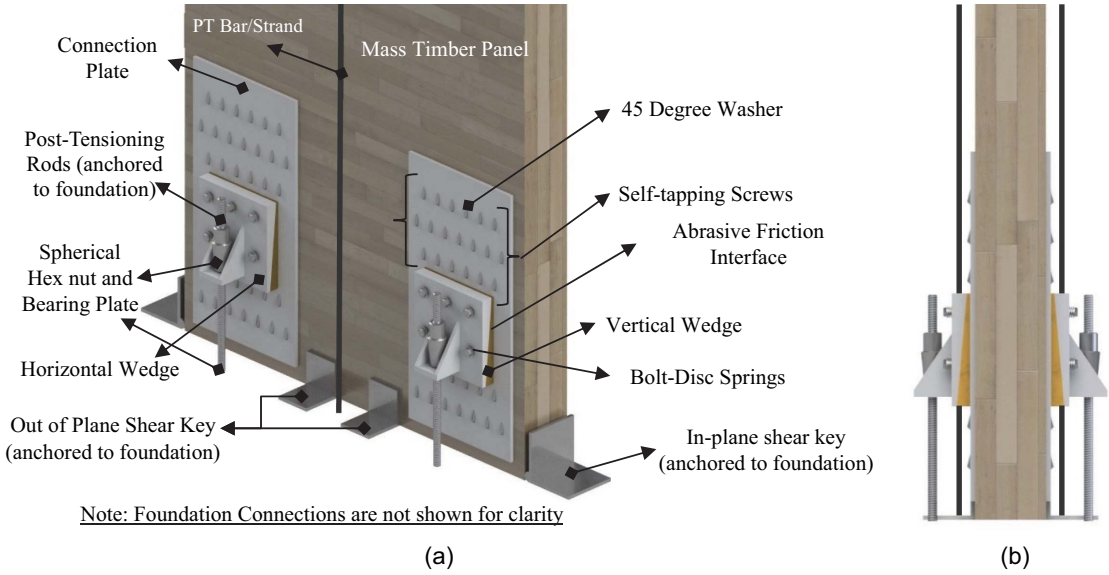

Fig. 1. UFD general schematic components: (a) side view; and (b) end view.

material type. With minor modifications, the friction dampers could also be adapted for any rigid rocking wall system of any material.

The friction force generated in the damper is generated through a normal clamping force provided by the high strength rods in combination with stacked disc-washers (i.e., referred to as the bolt–disc spring element). Some self-centering capability of this damper is provided through the detailing of an angled surface between the two contact surfaces of the sliding wedges in combination with the normal clamping force. This basic concept has been considered by others and shows high promise (Filiatrault et al. 2000; Hashemi et al. 2018). The bolt–disc spring element maintains a normal clamping force applied to the friction interface and represents a linear elastic spring of constant axial stiffness. Note that stacking disc springs (e.g., Belleville washers) in series increases the total horizontal displacement of the horizontal wedge, whereas stacking disc springs in parallel increases the clamping force of the bolt–disc spring component. The stacking configuration of the washers (i.e., parallel, series, or combination) will affect the stiffness of the bolt–disc spring component and provides the opportunity to "tune" the damper for a target performance. Considering the rocking motion of the PT-RMTW, the clamping force in the bolt–disc spring element increases by each increment of wall uplift to the point where all disc springs have reached their flattening force (to be avoided in design). The condition where all washers are flattened is the maximum horizontal travel of the wedges representing the maximum uplift displacement condition of the vertical wedge and PT-RMTW. Analytical equations and detailed presentation describing the basic kinematics of the UFD have been established based on first principles using simplified free body diagrams (FBDs) and presented in (Tatar and Dowden 2022).

Payload Shake-Table Test Setup

NHERI TallWood 10-Story Mass Timber Building

The mass timber 10-story test building designed by the TallWood project team incorporated a variety of combinations of different mass timber products. The gravity frame system consisted of a beam-column grid with veneer laminated timber (VLT) beams and columns. The floor/roof panels used various panel types along the height of the building consisting of CLT, Glue Laminated Timber, nail/dowel laminated timber, and VLT panels. The lateral system consisted of a pair of exterior post-tensioned rocking walls with VLT bounding columns in each orthogonal building direction (i.e., two rocking walls in each direction). The rocking walls in the north–south direction and east–west direction comprised of mass plywood panel (MPP) and CLT panels, respectively (see Figs. 2 and 3). Each of these rocking walls were post-tensioned with a total of four Simpson Strong-Tie ATS high strength steel rods anchored at the foundation level and the tops of the wall at the roof level. The first one and one-half stories used 50.8-mm (2 in.) diameter rods, and the remaining length along the height of the building used 31.75-mm (1.25 in.) diameter rods, where mechanical couplers were used at the transitions. An initial post-tensioning force of approximately 50% the yield strength of the PT rods was provided. Seismic energy dissipation was provided using U-flexural plate (UFP) steel yielding dampers detailed between the bounding column-to-wall connections at each level. A detailed description and lateral seismic design of the 10-story building is presented by (Pei et al. 2023, forthcoming; Wichman et al. 2022b). Tests were

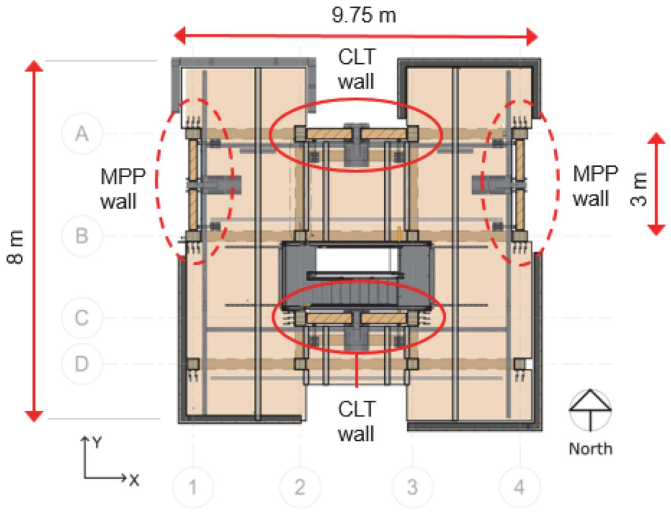

Fig. 2. Post-tensioned rocking walls. (Adapted from Busch 2023.)

(a) (b)

Fig. 3. MPP wall elevations: (a) west MPP wall; and (b) east MPP wall. (Images by Daniel M. Dowden.)

conducted at the NHERI shake table located at University of California San Diego.

Payload Test with UFDs

The payload shake table tests reported in this paper occurred after completion of the test program conducted by the NHERI TallWood project team. The objective of these payload tests was to validate the performance of the proposed UFDs subjected to simulated dynamic earthquake loads installed on rocking walls with realistic boundary conditions (Dowden and Tatar 2024). Given the existing design constraints of the 10-story building (previously established by the NHERI TallWood team), the UFDs were installed as added supplemental energy dissipation devices, whereas all other existing conditions of the test building remain unchanged. Furthermore, due to budgetary and time constraints, UFDs were installed on walls in only one primary direction. Because the UFDs were installed after the NHERI TallWood testing was finished, the MPP walls in the north–south direction were selected to avoid interference with the building's central stair core.

A 3D rendering of the fabricated UFDs is presented in Fig. 4(a). As highlighted in the figure, the UFDs comprise of two main components. The first components include the concrete filled hollow horizontal and vertical steel wedges fabricated with 12.7-mm (1/2 in.) thick grade 345 MPa (50 ksi) steel plates. Plastic plugs were 3D printed and installed prior to the concrete filling providing hollow block outs for the thru-rods. Detailing the wedges as hollow steel shells with concrete fill reduces the damper weight and eliminates the need for solid thick steel plates. In particular, depending on

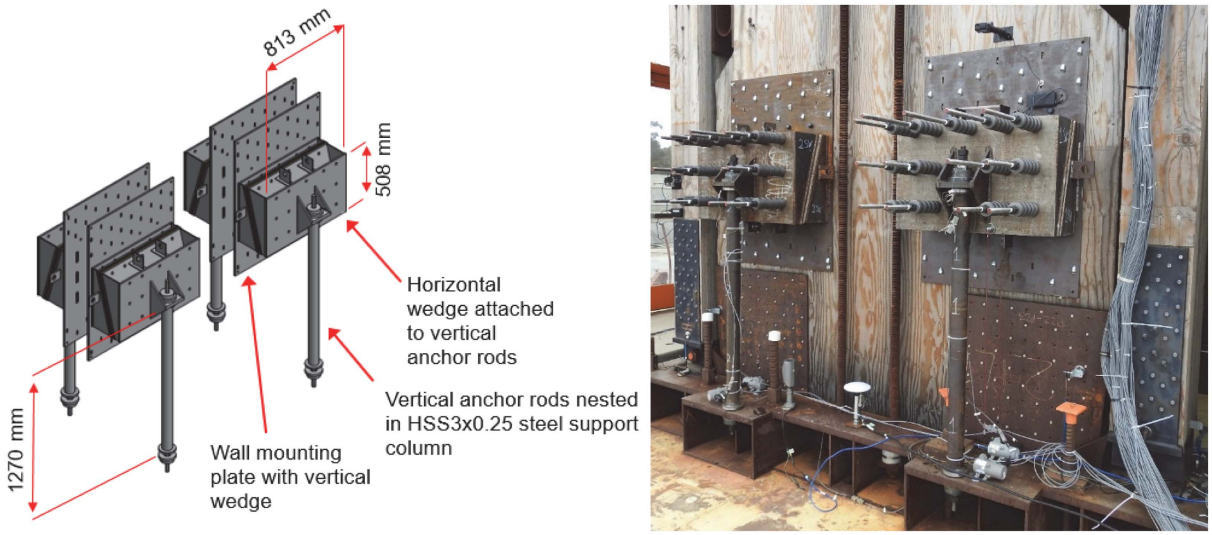

(a) (b)

Fig. 4. (a) UFD schematic; and (b) installed UFD at West MPP wall.

the angle of inclination of the friction interface referenced from vertical and the overall size of the friction wedges, the use of solid steel wedges could become unpractical. For the dampers used in these tests, the angle of inclination referenced from a vertical axis of the inclined friction surface was 15°. The vertical wedge is welded to the steel wall mounting plate, and this assembly is attached to the MPP walls with Simpson Strong-Tie (SDCF221334) 45° oriented 8 × 349-mm (0.315 × 13.75 in.) self-tapping screws. The second components include the 25.4-mm (1 in.) diameter Simpson Strong-Tie ATS-HSR8 vertical anchor tension rods nested inside HSS76.2 × 6.35 (HSS3 × 0.25) steel pipe columns. In this assembly, the tension rods anchor the horizontal wedges to the foundation and the HSS steel pipe column supports the weight of the concrete-filled steel horizontal wedges and ensures the horizontal wedges remain essentially at the same elevation as the vertical wedges slide against the horizontal wedges during wall rocking. Furthermore, the connections at the top and bottom of the pipe column/tension rod assemblies were attached to the foundation beam and the horizontal wedge with spherical plate washers to allow unrestrained rotation at these connection points. A finished installed damper is presented in Fig. 4(b) shown at the exterior face of the West MPP wall.

Furthermore, the friction materials used 12.7-mm (1/2 in.) thick leaded-tin-bronze (LTB) and stainless steel (SS) plates. The LTB plates consisted of a C93200 alloy plate and were attached to the horizontal wedges. The SS plate consisted of type 410 plate and attached to the vertical wedges. The friction plates were attached to the UFD wedges with 13 12.7-mm (1/2 in.) diameter threaded steel cap screws. The damper components on opposite faces of the MPP wall were tied together with 19-mm (3/4 in.) diameter Simpson Strong-Tie ATS-HSR6 tension thru-rods. To provide the clamping force needed to develop friction forces between the horizontal and vertical wedge interfaces, steel disc-washers (disc-springs) with a conical disc height to thickness ratio (h/t) of 0.57 were used at each end of the thru rods. The stacking configuration consisted of a parallel series of 6 disc-washers stacked in parallel (i.e., nested) and each nested bundle placed in series 10 times. This stacking configuration provided an axial spring stiffness of approximately 175 kN/m (31.4 kip/in.) per thru rod. A view of the vertical wedge with SS friction plate, horizontal wedge with LTB friction plate, installed wedges, and connection detail at the top and bottom of the nested tension anchor rod/support column is presented in Fig. 5.

These tests are essentially a continuation of shake-table testing beyond the NHERI TallWood project tests, but with UFDs installed at the base of the MPP rocking walls. Accordingly, all existing instrumentation from the NHERI TallWood team's tests were left in place and used for these tests. For information on this installed instrumentation see (Busch 2023; Pei et al, forthcoming; Wichman 2023). For each UFD, 12 sensors were added at each damper location to monitor forces and displacements for a total of 48 additional instrumentation sensors added to the test building. A total list of added instrumentation is summarized in Table 1. A typical sensor placement on one side of the UFD is presented in Fig. 6. Instrumentation sensors included load washers (i.e., load cells) at 5 of the 13 thru rods per UFD, a load washer at each uplift tension rod, a vertical oriented string potentiometer at each horizontal and vertical wedge, and a horizontal oriented string potentiometer on the horizontal wedges located inside of the building. Lastly, with the instrumentation installed, the thru rods were each post-tensioned to an initial rod clamping force ranging between approximately 13.3 and 22.2 kN (3 and 5 kips). All instrumentation data was collected at a sample rate of 256 Hz.

Testing Program and Select Experimental Results

Testing Program

The shake-table test program consisted of 10 earthquake tests. Furthermore, to determine natural frequencies and quantify changes in dynamic properties of the building, white noise (i.e., an acceleration-controlled flat-spectrum broadband random motion) identification tests were also conducted. Given that these payloads tests are essentially an extension of the NHERI TallWood tests but with the added friction dampers installed, ground motion (GM) selections for the tests were based on a predefined suite of GMs established by and previously used by the NHERI TallWood team in their testing program. This process was necessary because these GMs were already tuned for the shake-table drive control and scaled to various target seismic hazard levels specific for the 10-story building design. A detailed presentation on the ground motion scaling and development of GMs used in these tests can be found at (Pei et al., forthcoming; Wichman 2023). Furthermore, repeating select GMs used by the NHERI TallWood team also provided an opportunity to compare building response with and without the UFD dampers for a given earthquake test. For these tests, five different historical earthquake accelerograms were selected each with a different scaled seismic hazard [i.e., 225, 475, 975, and 2475 (MCE_R) year return periods]. Because the UFDs were installed only in the north–south orientation (Y-direction), typically the earthquake tests were performed with only the Y-component (horizontal) or combination of the Y and Z (vertical) components of the accelerograms. A summary of the test plan is presented in Table 2.

Experimental Results—White Noise

White noise tests were conducted to identify the dominant modes of vibration of the test building and are indicated with WN in Table 2. Period elongation observed between white noise runs can also indicate occurrence of structural damage during the earthquake tests. The white noise transfer functions at the roof level are presented in Fig. 7 for the building condition before testing and upon completion of testing. Note that the first three modes dominate and that the building did not have a noticeable change of period over the progression of earthquake testing, indicating that damage was likely minimal.

Experimental Results—Global Response

The global response performance of the building is assessed by base shear, peak floor accelerations, and peak interstory drifts. Select response plots quantifying these parameters are presented subsequently. Furthermore, for brevity, only results from the Loma Prieta ground motion are reported because it represents the MCE_R level scaled earthquake test leading to the most extreme demands on the test building. The base shear was calculated as the summation of story forces that were obtained as the total acceleration response measured from accelerometers at each story level, multiplied by the calculated mass at that level. For this purpose, accelerometers installed at the approximate center of mass at each floor level were used to calculate these forces. Furthermore, the raw acceleration data was modified using a band pass filter with cutoff frequencies ranging from 0.10 to 0.12 Hz and 50 Hz. Additionally, given the height of the test building, string potentiometers to measure building level displacements could only be installed up to floor level 4. Consequently, floor/roof level displacements along the building height used to obtain the interstory drifts were calculated through numerical double integration of the response history data

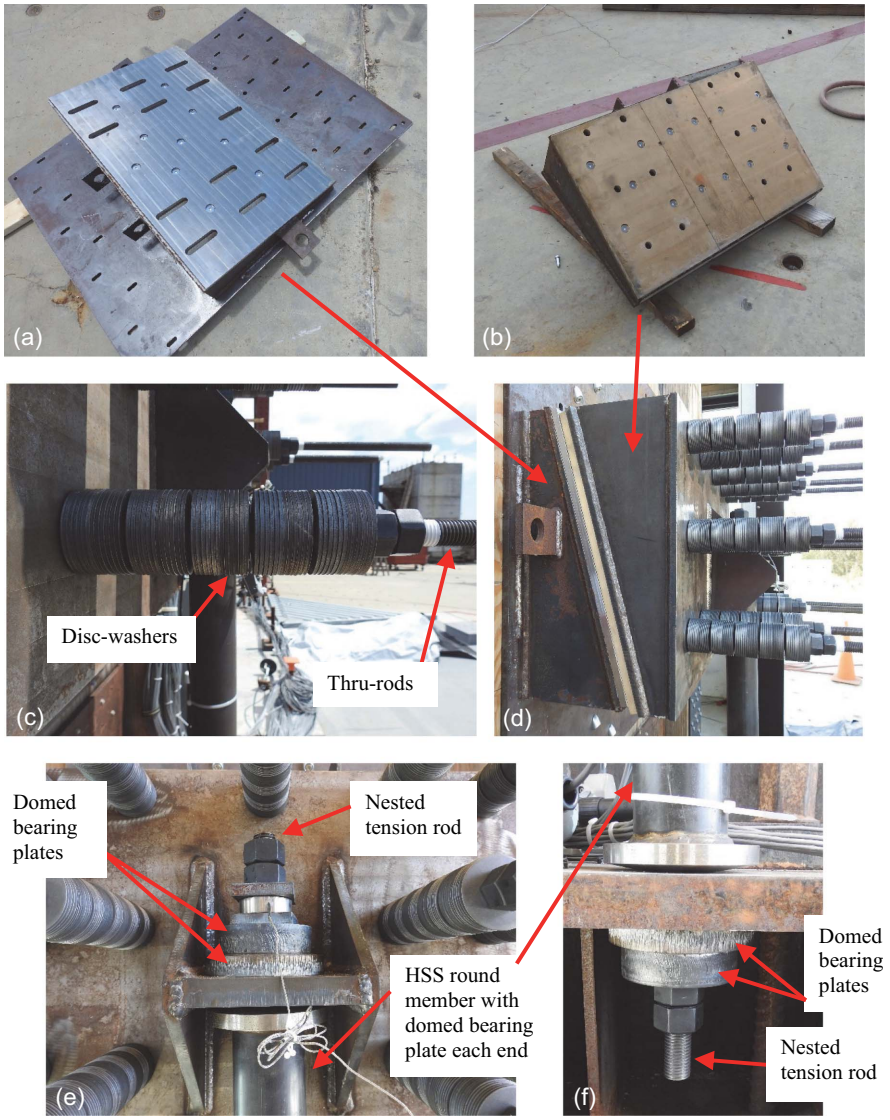

Fig. 5. UFD parts: (a) vertical wedge with SS friction plate; (b) horizontal wedge with LTB friction plate; (c) installed disc washers; (d) installed UFD; (e) top of tension anchor rod; and (f) bottom of tension anchor rod.

Table 1. Additional instrumentation for UFDs

UFD component	Sensor types	Total number
Vertical wedges	SP	8
Horizontal wedges	SP	12
Through rods	LW	20
Uplift tension rods	LW	8

Note: SP = string potentiometers; and LW = load washers.

collected by the accelerometers. The frequency band noted was selected to ensure all dominant modes were included informed by the white-noise tests transfer functions that showed the dominant frequencies. Furthermore, because string potentiometers were installed at levels 2–4 and could be used for comparison, the filtered frequency band noted was also informed by minimizing the root-mean-square error of the measured (from string pots) and estimated (integrated) level displacement response history. A comparison of the integrated acceleration displacements overplotted with the string potentiometers located at the SW and SE corners of floor level 4 is presented in Fig. 8, and they are in excellent agreement. The global response data presented in Figs. 9–13 support the following observations:

1. The hysteretic response presented in Fig. 9 provides an indicator of energy dissipation and global behavior. Furthermore, the peak base shear was determined to be approximately 890 kN (200 kips). The total seismic weight of the building was calculated to be 2,718 kN (611 kips). For perspective, the base shear normalized by the total seismic weight can be rewritten in terms of the gravity constant as 0.33 g and serves as a proxy for the MCE level base shear coefficient for this test.
2. The peak roof drift was measured to be 1.57%, which is below the 2% code drift limit. This observation supports the assertion that the design methodology the NHERI TallWood team used to design the 10-story building satisfied this code-based design parameter.
3. An envelope of the minimum, maximum, and peak story force and shears is presented in Fig. 10. The maximum story force occurred near the mid-height of the building at Level 6. Additionally, absolute story force peaks (shown by the solid data

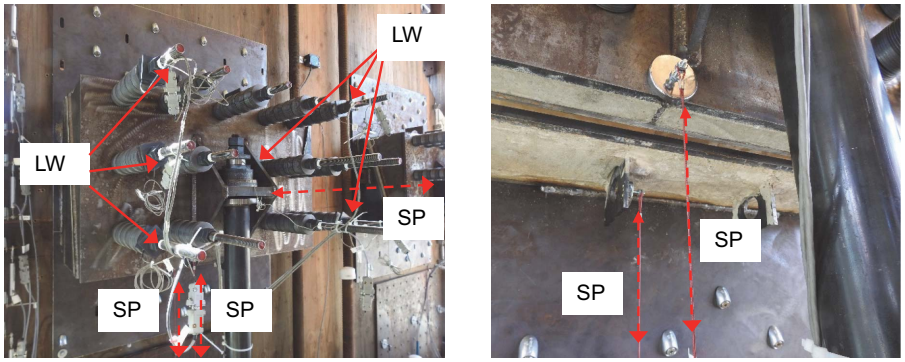

Fig. 6. Instrumentation placement: (a) overview; and (b) bottom of UFD.

Table 2. Test plan

Test ID	Hazard level	Direction	Earthquake name	Total duration (s)	Achieved input PGA (g)		
					X	Y	Z
WN	—	X	—	—	—	—	—
WN	—	Y	MID101_WN_Y	—	—	—	—
1[a]	225	Y	Nigata, Japan	75.0	—	0.354	—
2	225	YZ	Nigata, Japan	78.3	—	0.368	0.096
3[a]	475	Y	Chi-Chi	79.5	—	0.298	—
4	475	YZ	Chi-Chi	—	—	0.287	0.364
WN	—	X	—	—	—	—	—
WN	—	Y	—	—	—	—	—
5[a]	975	Y	Northridge-01	62.6	—	0.411	—
6	975	YZ	Northridge-01	63.6	—	0.411	0.263
WN	—	X	—	—	—	—	—
WN	—	Y	—	—	—	—	—
7	975	YZ	Victoria, Mexico	48.7	—	0.528	0.336
WN	—	X	—	—	—	—	—
WN	—	Y	—	—	—	—	—
8	MCE_R	Y	Loma Prieta	61.5	—	0.795	—
WN	—	X	—	—	—	—	—
WN	—	Y	—	—	—	—	—
9	475	X	Chi-Chi	74.3	0.463	—	—
10[a]	475	XYZ	Chi-Chi	79.4	0.458	0.262	0.352
WN	—	X	—	—	—	—	—
WN	—	Y	MID110_WN_Y	—	—	—	—

[a]Exact repeat of NHERI TallWood Team's Phase I tests.

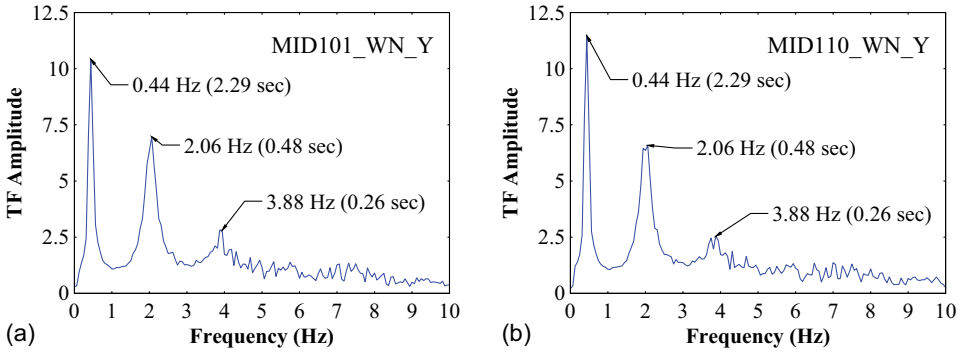

Fig. 7. Roof level white noise response: (a) pretesting; and (b) post-testing.

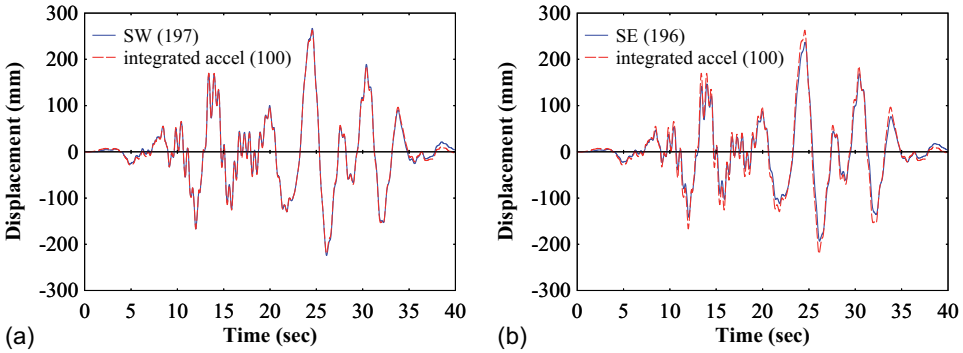

Fig. 8. Loma Prieta (MCE_R); level 4 displacement check: (a) SW corner; and (b) SE corner.

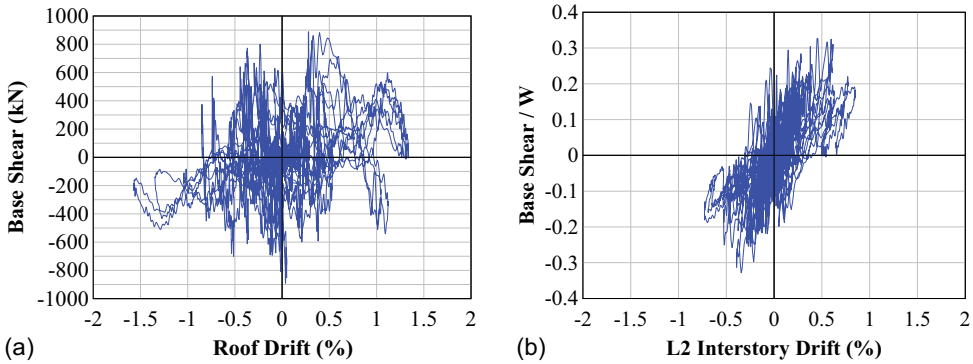

Fig. 9. Loma Prieta (MCE_R): (a) base shear versus roof drift; and (b) base shear coefficient versus level 2 interstory drift.

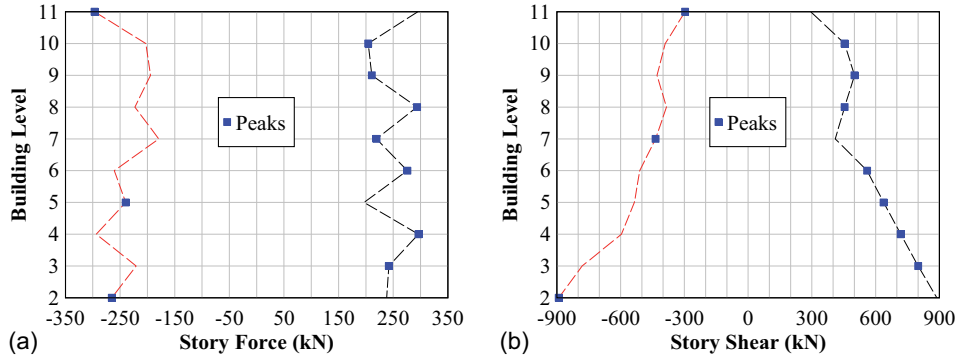

Fig. 10. Loma Prieta (MCE_R): (a) peak story force; and (b) peak story shear.

point markers) along the building height are similar in magnitude. Accordingly, the influence of higher mode effects is not insignificant.

4. An envelope of the minimum, maximum, and peak interstory drifts and accelerations are presented in Fig. 11. The dashed lines represent the maxima and minima, whereas the solid data point markers follows the absolute peaks along the height of the building. As observed, the peak interstory drift occurred at level 10 with a measured value of 2.33%. Furthermore, the peak level acceleration was measured at 1.26 g and occurred at the roof level. The next largest peak acceleration occurred at floor level 6 with a recorded peak acceleration of 1.13 g. From the envelope of peak interstory drifts and accelerations, the influence of higher mode effects is apparent from the distribution of peaks.
5. To validate the building's self-centering response, the approximate residual level displacements are presented in Fig. 12(a) with a maximum value of 5.3 mm observed at level 7. The vertical dashed lines in the figure represent the out-of-plumb acceptable tolerance of $h/500$ that is commonly used as a metric to assess recentering. The building is well within these bounds and can be considered fully recentered. To provide further evidence of building recentering, Fig. 12(b) shows the approximate total PT force response history of the MPP wall measured from installed load washers. The PT force at the beginning and at the

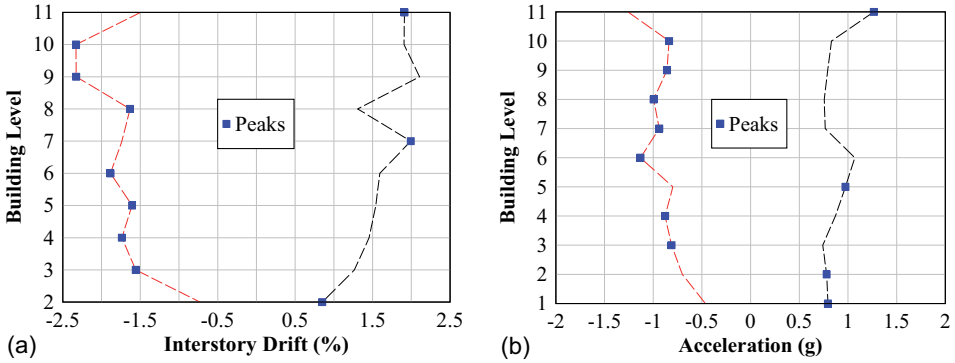

Fig. 11. Loma Prieta (MCE_R): (a) peak interstory drifts; and (b) peak level accelerations.

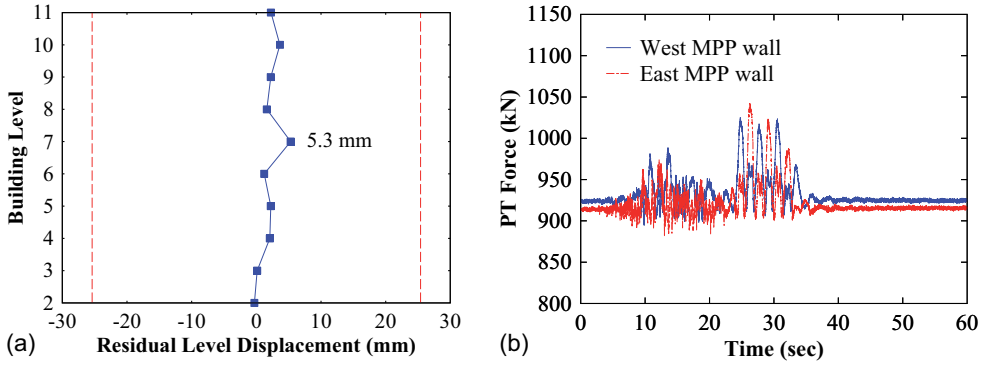

Fig. 12. Loma Prieta (MCE_R): (a) residual displacement; and (b) PT response history.

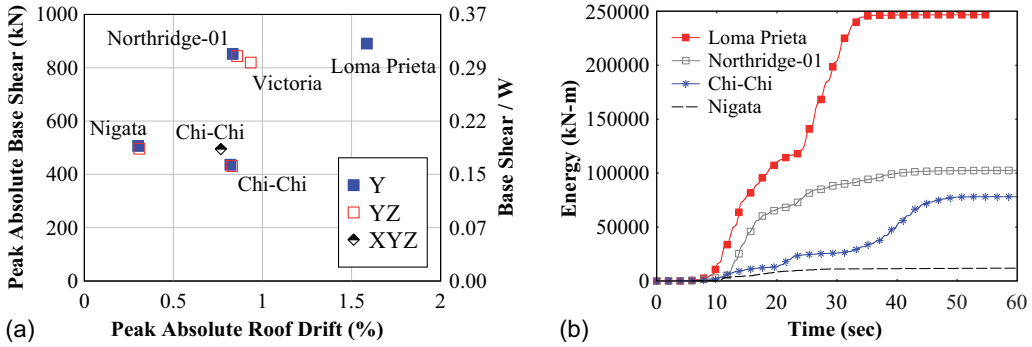

Fig. 13. Comparison of building response: (a) all GMs; and (b) *y*-direction GMs.

end of the ground motion are the same, indicating that the MPP wall returned to its original position at the end of the earthquake test.

6. A summary comparison of the building response in terms of absolute base shear and roof drift peaks for the different ground motion tests is presented in Fig. 13(a). When comparing the results for the same GM with and without a vertical component, note that including the vertical component of the GM does not significantly influence the lateral response. However, for the case of Chi-Chi, the cross-coupling effect of including both the *x*- and *y*-components of the GM is apparent, where a 15% increase in base shear is observed.
7. A summary comparison of building response in terms of cumulative work energy is presented in Fig. 13(b) for GMs in the *y*-direction. This finding is quantified as the accumulated inertial force at each level multiplied by that level displacement (relative to ground) summed along the building height at each time step. As expected, Loma Prieta has the largest cumulative energy response. Additionally, observed in Fig. 13(a), it is interesting to note that Chi-Chi (*y*) had a lower peak base shear than Nigata (*y*) given that Chi-Chi was scaled to a larger seismic hazard. However, Fig. 13(b) shows that Chi-Chi did have a significantly larger energy response corroborating the higher seismic intensity then Nigata.

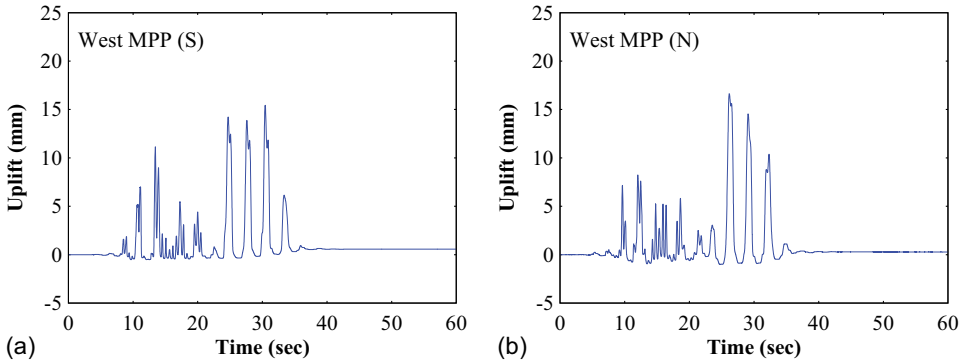

Fig. 14. Loma Prieta (MCE_R) West MPP wall uplift: (a) south end; and (b) north end.

Experimental Results—UFD Response

The UFD dampers are displacement controlled and are dependent on wall rocking behavior to produce wall uplift. To monitor wall uplift at the toe of the rocking walls, linear potentiometers were installed at these locations at each exterior and interior wall faces. Furthermore, the force response of the UFDs was obtained with 222 kN (50 kip) and 445 kN (100 kip) load washers installed on the thru rods and uplift tension rods, respectively. Each UFD was detailed with 13 thru rods; however, only load washers on 5 of the 13 rods at each UFD location were installed due to budgetary constraints. Accordingly, the results presented subsequently assume an average tension force per thru rod based on the average of the 5 load washers at each UFD location. Conversely, load washers were installed at all the uplift tension rods (i.e., eight locations). However, note that the uplift tension rod load washer at the north end of the west MPP wall, at the interior facing wall location, was damaged during instrumentation installation, so no data was collected on that sensor. The response plots presented subsequently support the following observations:

1. The average of the measured uplifts at opposite faces of the walls (i.e., interior and exterior) at a wall rocking toe location is presented in Fig. 14 for the West MPP wall. As observed, the MPP walls did experience wall rocking. The peak average uplift was measured at 15.4 mm (0.61 in.) and 16.6 mm (0.65 in.) at the south and north ends of the MPP wall, respectively.
2. The hysteresis response of the damper 1 (i.e., south end of the west MPP wall) is presented in Fig. 15(a) in terms of the axial tension force measured in the uplift anchor rods and the net vertical displacement between the horizontal and vertical wedges. The latter was obtained as the difference between the measured displacement between the vertical string potentiometers attached to the respective vertical and horizontal wedges and represents the relative sliding motion between the UFD wedges. The following observations can be made:
   a. The UFDs are providing energy dissipation through the presence of hysteresis loops. Compared with a rectangular hysteresis curve of flat slider friction devices, the differences in shape of the UFD hysteresis response observed here are due to the use of the combination of inclined friction interfaces and use of disc washers to provide the normal clamping forces. This has the effect of leading to a tapered rectangular hysteresis loop(s). However, as will be shown subsequently, the shape of this hysteresis is atypical because there is a noticeable "pinching" effect as the damper returns to its initial position. It is speculated that this pinching is due to some binding effects resulting from installation.
   b. The hysteresis response is not fully symmetrical on each side of the UFD (as would be expected for analytical and numerical models that assume idealized behavior of the UFD wedges as rigid blocks). This finding suggests that some differences can be expected due to installation fit-up (e.g., leading to binding from other sources of friction within the actual connection), differences in surface conditions within same friction plates (e.g., local as-delivered surface variations within the SS plates and LTB plates), and differences in forces in the tension anchor rods (on account of the aforementioned).
   c. The net vertical displacement peaks between the west and east sides of the UFD do not match. The net vertical displacement is larger for the SE side of the UFD compared with the SW side. This finding suggests that some unbalance of the

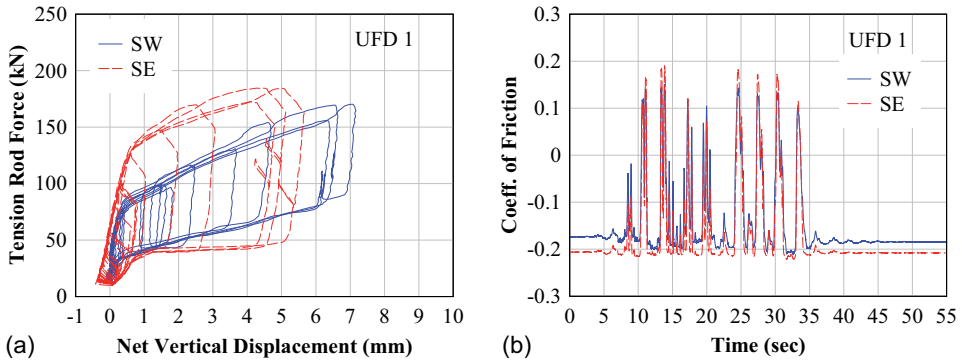

Fig. 15. Loma Prieta (MCE_R): (a) global UFD 1 response; and (b) COF response.

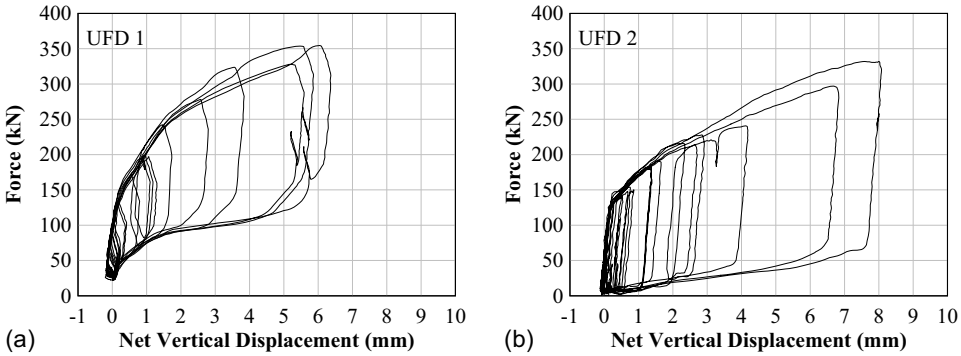

Fig. 16. West MPP wall UFD total response: (a) south end; and (b) north end.

wedges on opposite sides of the UFD can occur. However, the difference between the peak is approximately 1.5 mm (0.06 in.), which is a relatively small difference and does not appear to have any detrimental effects on the damper performance.

3. The coefficient of friction (COF) can be calculated through static force equilibrium of either the horizontal or vertical wedges with the measured horizontal clamping force (F) and the corresponding measured tension force (T) in the uplift anchor rods leading to Eq. (1), where θ is the sliding interface angle of the two wedges referenced from the vertical. Accordingly, the calculated COF response history for damper 1 is presented in Fig. 15(b). At the southwest (SW) side of damper 1, the COF was determined to be in the range between 0.15 and $(-)0.21$ with an averaged value of 0.18. At the southeast (SE) side of damper 1, the COF was determined to be in the range between 0.19 and $(-)0.22$ with an averaged value of 0.20. Note that the negative sign on the COF reflects the sign on the friction force (since the COF cannot actually be negative). For the condition when the tension force (T) in the uplift anchor rods is smaller than the horizontal clamping force (F), the directionality of the friction force value will be negative (resulting in the negative sign shown for the COF). Furthermore, the time history of the COF will vary because T and F will vary depending on the vertical rocking movement of the wall

$$\mu = \frac{T\cos\theta - F\sin\theta}{F\cos\theta + T\sin\theta} \tag{1}$$

4. The total uplift force versus net average vertical displacement at each of the UFDs is presented in Figs. 16 and 17. As observed in Fig. 15(a), the pinching effect at UFD 2 to UFD 4 dampers is not present and is more in line with the expected hysteretic response (Tatar and Dowden 2022). Additionally, the net vertical displacement returns to essentially zero, indicating that there is negligible residual relative displacement between the two wedges of the UFD at the end of the earthquake test.
5. An example of the in-plane (i.e., flat-slider) response along the interface of the UFD wedges is presented in Fig. 18 for the SW side of UFD 3. In this orientation, the friction response is represented as would be observed for a flat slider characterized by the essentially rectangular hysteresis. Furthermore, the COF ranges between 0.13 and $(-)0.26$ at this location with an averaged value of 0.195.

Experimental Results–Influence of UFDs

The UFDs were added to the base of the MPP walls as supplemental energy dissipation devices. To quantify the added effect of the UFDs on global response of the building detailed with the UFPs, select repeat GM tests that the NHERI TallWood team conducted without the UFDs installed were conducted to provide some comparison. For this purpose, Test IDs 1 (Nigata), 3 (Chi-Chi), and 5 (Northridge-01) with y-component listed in Table 2 are only applicable given that UFDs were installed on the MPP walls only. Furthermore, for brevity, only comparisons with Northidge-01 are presented because it represents the highest seismic hazard level of these GMs. The subsequent response plots support the following observations:

1. The absolute peak base shear, absolute peak roof drift, and cumulative total work-energy of the building is compared in Fig. 19. From these plots, it is validated that the UFDs contributed to added energy dissipation and lateral resistance to the building response.

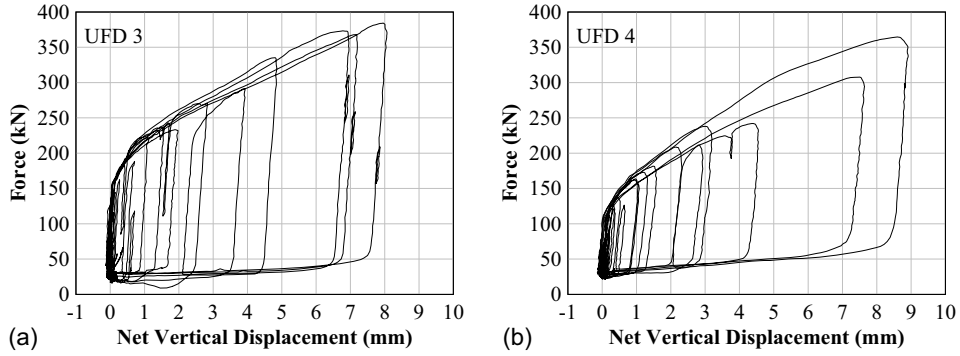

Fig. 17. East MPP wall UFD total response: (a) south end; and (b) north end.

J. Struct. Eng., 2025, 151(1): 04024199

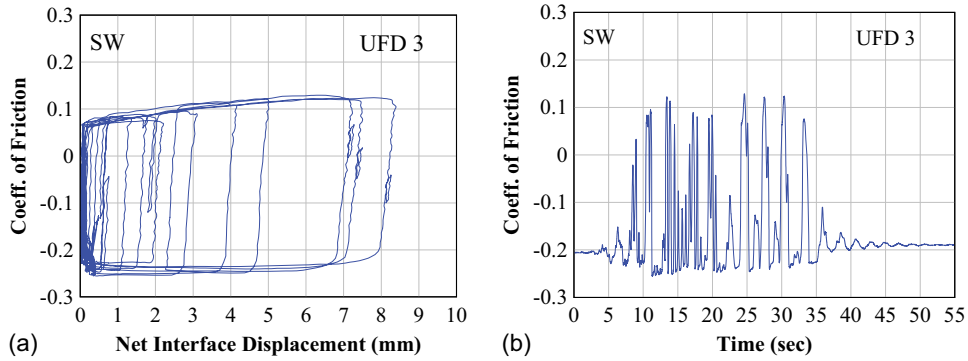

Fig. 18. In plane response—UFD 3.

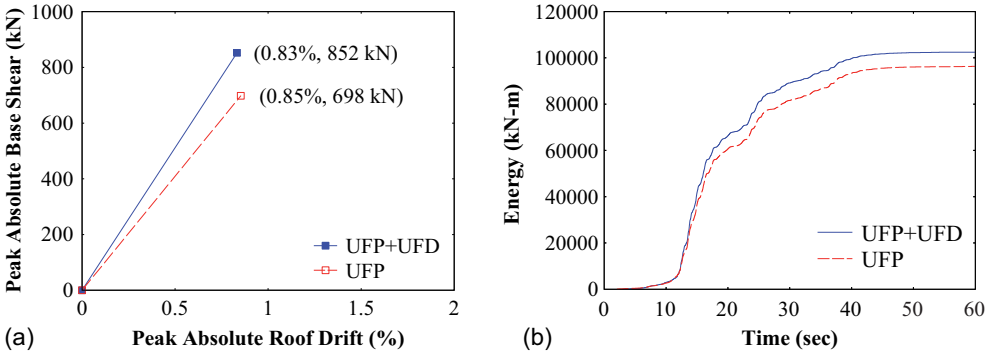

Fig. 19. Northridge-01 (Y): (a) peak response; and (b) cumulative energy dissipation.

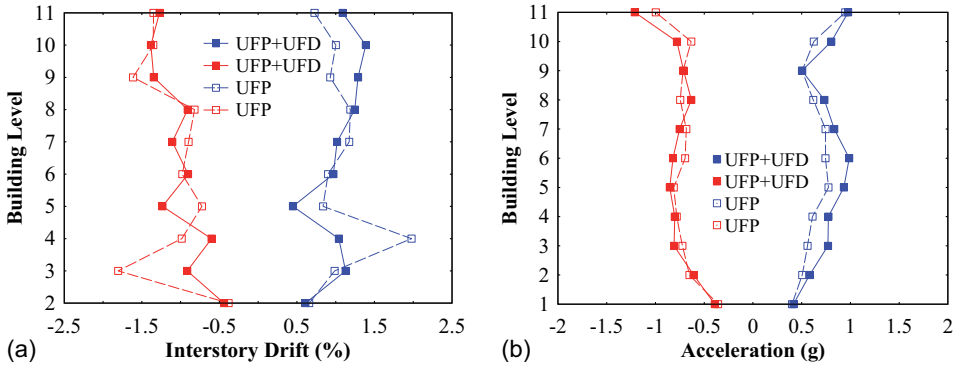

Fig. 20. Northridge-01(Y) building peak response: (a) interstory drift; and (b) acceleration.

2. The influence of the UFDs on peak interstory drifts is presented in Fig. 20(a). Note that the UFDs have a noticeable effect in reducing the peak interstory drifts near the bottom of the building where the UFDs were installed. Particularly, at Level 3, the peak negative drift response was reduced from 1.8% to 0.91%. At Level 4, the peak positive drift response was reduced from 1.98% to 1.04%. Given that the UFDs are installed at the bottom of the wall, it appears that the UFDs added some dynamic stiffness to the building system.
3. The influence of the UFDs on peak level accelerations is presented in Fig. 20(b). Although there is a small increase in peak accelerations (more noticeable in the positive direction), the overall effect on accelerations is not significant. However, because the peak accelerations tend to increase with the UFDs installed, it also provides evidence that the UFDs provide some additional stiffness to the building system.

Experimental versus Numerical Select Comparisons

A 3D numerical model for nonlinear response history analysis (NRHA) was developed in OpenSees (McKenna et al. 2010) to predict select global building response in preparation for the payload shake-table tests. The 3D numerical model parameters (e.g., seismic mass, center of mass, damping ratio, material properties, etc.) and

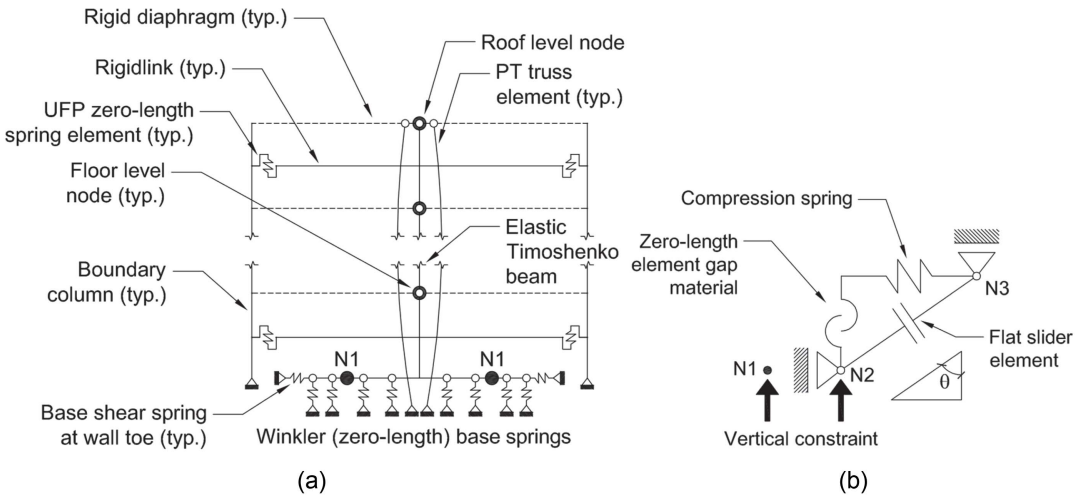

Fig. 21. OpenSees numerical model: (a) PT-RMTW; and (b) UFD.

modeling methods were provided by (Wichman 2023). A 2D schematic of the numerical model for one of the typical PT-RMTW is presented in Fig. 21(a) and is based on models previously adopted by other researchers (Ganey et al. 2017; Kovacs and Wiebe 2019; Wichman 2023). The difference here is that the numerical model of the UFD is now included. A brief overview description of the OpenSees numerical model is presented subsequently, but a more detailed description of the 3D modeling of the 10-story building can be found in Wichman (2023). Note that when referred to, OpenSees-specific elements, materials, and other components are denoted by italics.

As shown in Fig. 21(a), the wall of the PT-RMTW is modeled with a series of *ElasticTimoshenkoBeam* elements, to account for axial, flexural, and shear deformations. The post-tensioning system was modeled with truss elements connected from the roof node to the base foundation of the wall. The base of the rocking wall was modeled with a row of Winkler springs (*zeroLength* elements), and to transfer the base shear to the foundation, two springs with very high stiffness were placed at each end of the *rigidLink* beam connecting the Winkler springs. The UFPs are modeled using *zeroLength* elements with Steel02 *uniaxialMaterial* and connected at the boundary column to wall interface with *rigidLink* elements. The UFDs are modeled with a *flatSliderBearing* element as shown in Fig. 21(b), where nodes N2 and N3 represent the vertical and horizontal wedges and are constrained in the horizontal and vertical directions, respectively. This flat sider bearing element is typically used for modeling horizontal friction sliders, where the normal force is provided through the gravity load of the structure. In this configuration, however, the bearing element is oriented downward at an angle θ, and the normal force is provided by the effect of a compression-only *zeroLength* element representing the bolt-disc springs. Additionally, a zero-length element is defined between nodes N2 and N3 with an *ElasticPPGap* material, defined as having a gap equal to the slotted hole length of the vertical block of the UFD and with a high stiffness. Therefore, when vertical movement (i.e., wall uplift) of node N2 reaches to the end of the gap (equivalent to the vertical travel of through-bolts in the slotted hole of the vertical wedge), the gap element resists the uplift (which should be avoided in design). Finally, the resultant vertical damper forces are transferred to the PT-RMTW through an *equalDOF* constraint on the vertical wedge node.

For comparisons of predicted (numerical) to measured (experimental), select results of the Loma Prieta ground motion scaled to the MCE_R test are presented (representing the GM with the largest intensity). The as-recorded acceleration history from this test was used as the input GM in the NRHA. For reference, the recorded ground motion and the corresponding calculated response spectra acceleration are presented in Fig. 22. The response acceleration spectrum is based on a damping ratio of 6%. This finding was informed by Wichman (2023), who determined it to be the average damping ratio in the north–south direction obtained from the 10-story building free-vibration test data. Furthermore, in Fig. 22(b),

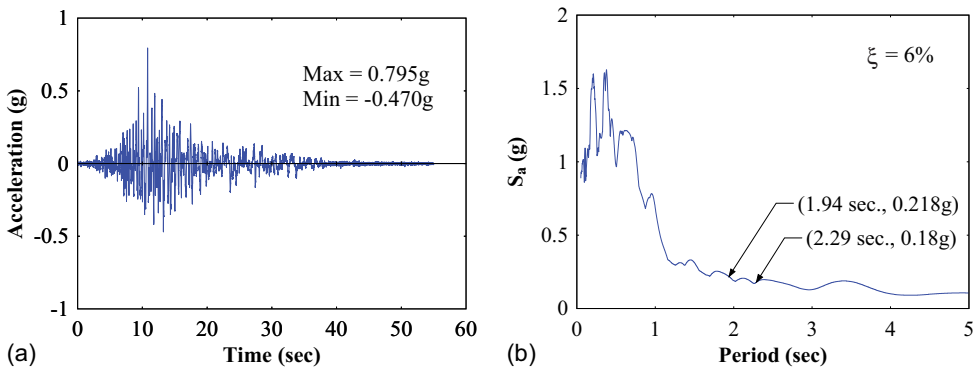

Fig. 22. Loma Prieta (MCE_R): (a) measured GM; and (b) spectral acceleration.

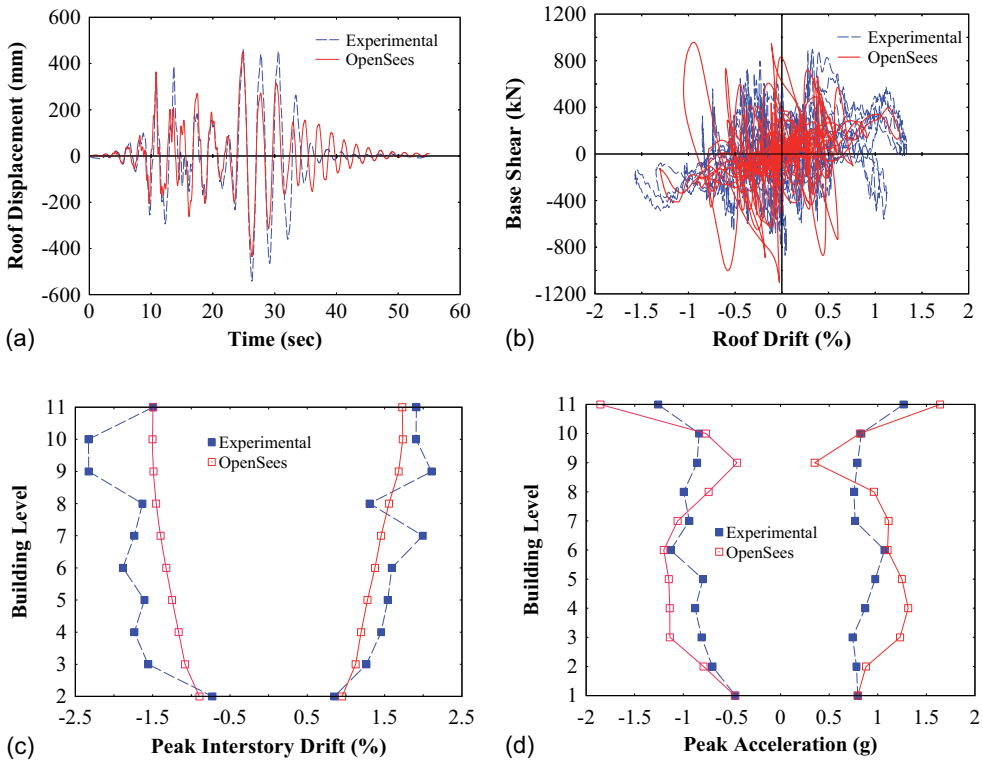

Fig. 23. Loma Prieta (MCE_R) experimental versus numerical: (a) roof displacement history; (b) base shear versus roof drift; (c) peak interstory drifts; and (d) peak level accelerations.

the fundamental mode period and the corresponding spectral acceleration is identified, where 1.94 s is the first mode period taken from the OpenSees eigen analysis, and the 2.29 s is that obtained from the experimental results (Fig. 7).

A comparison of select global building system response results of the numerical predictions with that of the measured experimental results is presented in Fig. 23. First, the roof displacement history is presented in Fig. 23(a). The maximum peak displacements are 460.4 mm (18.1 in.) and 450.1 mm (17.7 in.) for the experimental and numerical, respectively. The minimum peak displacements are −541.4 mm (−21.3 in.) and −435.8 mm (−17.2 in.) for the experimental and numerical results, respectively. Although the numerical and experimental do not track entirely on top of each other, the peaks occur at nearly the same time (26.3 and 24.8 s for negative and positive peaks, respectively), and the displacement history generally has a similar response, particularly during the portion of strong motion. Second, the base shear versus roof drift is presented in Fig. 23(b). The maximum peak base shears are 899 kN (202 kips) and 958 kN (215 kips) for the experimental and numerical results, respectively. Correspondingly, the minimum peak base shears are −870 kN (−196 kips) and −1,102 kN (−248 kips), respectively. The absolute peak base shear obtained from the numerical analysis overestimates the measured by approximately 23%. This difference can also be observed in the spectral acceleration at the fundamental period shown in Fig. 22(b), where the spectral acceleration at the fundamental period taken from the eigen analysis is approximately 21% larger than that at the period measured from the experimental results. Third, a summary of the peak interstory drifts is presented in Fig. 23(c). As observed, the OpenSees model underestimates the interstory drifts. Fourth, a summary of the peak level total accelerations is presented in Fig. 23(d), where it is observed that the numerical results overestimate the peak level accelerations. Furthermore, it is observed that the influence of higher mode effects is more pronounced in the numerical model.

Lastly, as observed in Fig. 23, there are some noticeable differences between the predicted numerical response compared with the measured experimental results. In part, this outcome can be attributed to differences between the actual 10-story building and the idealized numerical model. In particular, the numerical results assume only one ground motion effect and do not consider the cumulative inelastic effects due to the history of earthquake tests conducted by the NHERI TallWood team on the test building. Before this payload shake-table test program was conducted, the 10-story building was previously subjected to 100 earthquake ground motions, many of which were at a seismic hazard level between a 475-year return period to the MCE_R level earthquake intensity. Additionally, the numerical model does not include the nonstructural walls, exterior cladding, and the interior prefabricated steel stair system at the building's central core. Although these nonstructural components were detailed to be drift compatible with the building, their presence will have some influence on the building response. However, given these differences, generally the comparisons are within a reasonable order of magnitude.

Conclusion

The experimental results of a payload shake-table test program of the NHERI TallWood 10-story mass timber building were presented. These payload tests were conducted after the completion of the test program of the NHERI TallWood project. The primary objective of these additional tests was to validate the performance of a proposed uplift friction damper (UFD) solution for mass timber rocking wall seismic force-resisting systems subjected to simulated earthquakes on a test building with realistic boundary conditions.

A total of 10 earthquake tests of varying seismic hazard intensities, including an earthquake at the MCE_R level were conducted. For these payload tests, the UFDs were added to the base of the PT-RMTW in the N–S (y) direction as supplemental energy dissipation devices.

In comparison to the largest intensity select repeat GM test that the NHERI TallWood team conducted without the UFDs installed (i.e., Northridge-01), it was observed that the UFDs have a noticeable effect in reducing the peak interstory drifts near the bottom of the building where the UFDs were installed. Additionally, it was shown quantitatively that the UFDs contributed to added energy dissipation to the building response. Furthermore, upper bound measured results reported using the MCE_R ground motion (i.e., Loma Prieta) test showed that the post-tensioned mass timber rocking walls with the added UFDs exhibited excellent seismic performance. The peak system responses (i.e., base shear and interstory drifts) were within acceptable limits for an MCE_R level event. Moreover, the building fully recentered where the residual drifts were negligible. Lastly, some limited comparisons were provided with NRHA conducted using OpenSees. Given that the numerical model did not include the nonstructural components and only considered loading of one ground motion, the comparative results of the predicted (numerical) versus measured (experimental) were within a reasonable order of magnitude.

These tests provided further evidence of the seismic resiliency of the 10-story mass timber building designed by the NHERI TallWood project team. Structural damage was limited to the UFPs and functioned properly as structural fuses that could be replaced post-event without affecting the building's gravity frame system if deemed necessary in an actual significant earthquake scenario. Furthermore, these tests validated the performance of the UFDs subjected to earthquake loadings. The combination of UFP structural fuses attached to the boundary columns along the height of the building in parallel with the proposed UFDs attached to the base of the rocking walls was shown to be an effective combination, leveraging the full potential of the natural kinematics of the rocking walls (i.e., movement along the boundary column-to-wall interface and bottom of wall-to-foundation interface). The experimental results presented provide further evidence that tall mass timber buildings with post-tensioned rocking wall SFRSs is achievable.

Data Availability Statement

Some or all data, models, or code that support the findings of this study are available from the corresponding author upon reasonable request.

Acknowledgments

Funding for these payload tests was provided by the National Science Foundation under award numbers CMMI 2025449, 1634204, and 1636164. The first author would like to thank the NHERI TallWood team for their support in being part of this test program. Additionally, Simpson Strong-Tie donated all the threaded rods and self-tapping screw hardware for the damper installation. Thank you to Steve Pryor at Simpson Strong-Tie for assisting. Furthermore, the authors would like to thank Michigan Tech NSF REU student Alyssa Hill and graduate students Prashanna Mishra and Sir Lathan Wynn of the NHERI TallWood team for their help with installation of the dampers. Any opinions, findings, conclusions, and recommendations presented in this paper are those of the authors and do not necessarily reflect the views of the sponsors.

References

Akbas, T., R. Sause, J. M. Ricles, R. Ganey, J. Berman, S. Loftus, J. D. Dolan, S. Pei, J. W. van de Lindt, and H.-E. Blomgren. 2017. "Analytical and experimental lateral-load response of self-centering posttensioned CLT walls." *J. Struct. Eng.* 143 (6): 04017019. https://doi.org/10.1061/(ASCE)ST.1943-541X.0001733.

ASCE. 2017. *Minimum design loads and associated criteria for buildings and other structures*. ASCE/SEI 7-16. Reston, VA: ASCE.

Blomgren, H.-E., S. Pei, Z. Jin, J. Powers, J. D. Dolan, J. W. van de Lindt, A. R. Barbosa, and D. Huang. 2019. "Full-scale shake table testing of cross-laminated timber rocking shear walls with replaceable components." *J. Struct. Eng.* 145 (10): 04019115. https://doi.org/10.1061/(ASCE)ST.1943-541X.0002388.

Bruneau, M., and G. MacRae. 2017. *Reconstructing Christchurch: A seismic shift in building structural systems*. Christchurch, New Zealand: The Quake Centre, Univ. of Canterbury.

Busch, A. 2023. "Design and construction of tall mass timber buildings with resilient post-tensioned mass timber rocking walls." Ph.D. thesis, Dept. of Civil and Environmental Engineering, Colorado School of Mines.

Ceccotti, A., C. Sandhaas, M. Okabe, M. Yasumura, C. Minowa, and N. Kawai. 2013. "SOFIE project—3D shaking table test on a seven-story full-scale cross-laminated timber building." *Earthquake Eng. Struct. Dyn.* 42 (13): 2003–2021. https://doi.org/10.1002/eqe.2309.

Dowden, D. M., and A. Tatar. 2024. "Shake table test of a full-scale 10-story mass timber building with uplift friction dampers." In *Proc., 18th World Conf. on Earthquake Engineering*. Milan, Italy: World Conference on Earthquake Engineering.

Filiatrault, A., R. Tremblay, and R. Kar. 2000. "Performance evaluation of friction spring seismic damper." *J. Struct. Eng.* 126 (4): 491–499. https://doi.org/10.1061/(ASCE)0733-9445(2000)126:4(491).

Furley, J., J. W. van de Lindt, S. Pei, S. Wichman, H. Hasani, J. W. Berman, K. Ryan, J. Daniel Dolan, R. B. Zimmerman, and E. McDonnell. 2021. "Time-to-functionality fragilities for performance assessment of buildings." *J. Struct. Eng.* 147 (12): 04021217. https://doi.org/10.1061/(ASCE)ST.1943-541X.0003195.

Ganey, R., J. W. Berman, T. Akbas, S. Loftus, J. Daniel Dolan, R. Sause, J. Ricles, S. Pei, J. V. D. Lindt, and H.-E. Blomgren. 2017. "Experimental investigation of self-centering cross-laminated timber walls." *J. Struct. Eng.* 143 (10): 04017135. https://doi.org/10.1061/(ASCE)ST.1943-541X.0001877.

Gavric, I., M. Fragiacomo, and A. Ceccotti. 2015. "Cyclic behavior of CLT wall systems: Experimental tests and analytical prediction models." *J. Struct. Eng.* 141 (11): 04015034. https://doi.org/10.1061/(ASCE)ST.1943-541X.0001246.

Green, M., and E. Karsh. 2012. *The case for tall wood buildings*. North Vancouver, BC, Canada: Canadian Wood Council.

Hashemi, A., P. Zarnani, R. Masoudnia, and P. Quenneville. 2018. "Experimental testing of rocking cross-laminated timber walls with resilient slip friction joints." *J. Struct. Eng.* 144 (1): 04017180. https://doi.org/10.1061/(ASCE)ST.1943-541X.0001931.

Hristovski, V., B. Dujic, M. Stojmanovska, and V. Mircevska. 2013. "Full-scale shaking-table tests of XLam panel systems and numerical verification: Specimen 1." *J. Struct. Eng.* 139 (11): 2010–2018. https://doi.org/10.1061/(ASCE)ST.1943-541X.0000754.

IBC (International Building Code). 2015. *International building code*. Falls Church, VA: International Code Council.

Iqbal, A., S. Pampanin, A. Palermo, and A. Buchanan. 2015. "Performance and design of LVL walls coupled with UFP dissipaters." *J. Earthquake Eng.* 19 (3): 383–409. https://doi.org/10.1080/13632469.2014.987406.

Izzi, M., A. Polastri, and M. Fragiacomo. 2018. "Modelling the mechanical behaviour of typical wall-to-floor connection systems for cross-laminated timber structures." *Eng. Struct.* 162 (May): 270–282. https://doi.org/10.1016/j.engstruct.2018.02.045.

Kelly, J. M., R. Skinner, and A. Heine. 1972. "Mechanisms of energy absorption in special devices for use in earthquake resistant structures." *Bull. N. Z. Soc. Earthquake Eng.* 5 (3): 63–88. https://doi.org/10.5459/bnzsee.5.3.63-88.

Kovacs, M. A., and L. Wiebe. 2019. "Controlled rocking CLT walls for buildings in regions of moderate seismicity: Design procedure and numerical collapse assessment." *J. Earthquake Eng.* 23 (5): 750–770. https://doi.org/10.1080/13632469.2017.1326421.

Kramer, A., A. R. Barbosa, and A. Sinha. 2016. "Performance of steel energy dissipators connected to cross-laminated timber wall panels subjected to tension and cyclic loading." *J. Struct. Eng.* 142 (4): E4015013. https://doi.org/10.1061/(ASCE)ST.1943-541X.0001410.

Liu, J., and F. Lam. 2019. "Experimental test of coupling effect on CLT hold-down connections." *Eng. Struct.* 178 (Jan): 586–602. https://doi.org/10.1016/j.engstruct.2018.10.063.

Loo, W. Y., P. Quenneville, and N. Chouw. 2016. "Rocking timber structure with slip-friction connectors conceptualized as a plastically deformable hinge within a multistory shear wall." *J. Struct. Eng.* 142 (4): E4015010. https://doi.org/10.1061/(ASCE)ST.1943-541X.0001387.

Maurya, A., M. R. Eatherton, R. Matsui, and S. H. Florig. 2016. "Experimental investigation of miniature buckling restrained braces for use as structural fuses." *J. Constr. Steel Res.* 127 (Dec): 54–65. https://doi.org/10.1016/j.jcsr.2016.07.019.

McKenna, F., M. H. Scott, and G. L. Fenves. 2010. "Nonlinear finite-element analysis software architecture using object composition." *J. Comput. Civ. Eng.* 24 (1): 95–107. https://doi.org/10.1061/(ASCE)CP.1943-5487.0000002.

Pei, S., et al. Forthcoming. "Shake table testing of a full-scale ten-story resilient mass timber building." *J. Struct. Eng.* https://doi.org/10.1061/JSENDH/STENG-13752.

Pei, S., D. Huang, J. W. Berman, and S. K. Wichman. 2021. "Simplified dynamic model for post-tensioned cross-laminated timber rocking walls." *Earthquake Eng. Struct. Dyn.* 50 (3): 845–862. https://doi.org/10.1002/eqe.3378.

Pei, S., J. W. van de Lindt, A. R. Barbosa, J. W. Berman, E. McDonnell, J. Daniel Dolan, H.-E. Blomgren, R. B. Zimmerman, D. Huang, and S. Wichman. 2019. "Experimental seismic response of a resilient 2-story mass-timber building with post-tensioned rocking walls." *J. Struct. Eng.* 145 (11): 04019120. https://doi.org/10.1061/(ASCE)ST.1943-541X.0002382.

Pei, S., J. W. van de Lindt, J. Berman, K. Ryan, J. D. Dolan, S. Pryor, S. Wichman, A. Busch, and R. Zimmerman. 2023. "Full-scale 3-D shake table test of a ten-story mass timber building." In *Proc., World Conf. on Timber Engineering*. Olso, Norway: World Conference on Timber Engineering.

Pei, S., J. W. van de Lindt, M. Popovski, J. W. Berman, J. D. Dolan, J. Ricles, R. Sause, H. Blomgren, and D. R. Rammer. 2016. "Cross-laminated timber for seismic regions: Progress and challenges for research and implementation." *J. Struct. Eng.* 142 (4): E2514001. https://doi.org/10.1061/(ASCE)ST.1943-541X.0001192.

Polastri, A., I. Giongo, A. Angeli, and R. Brandner. 2018. "Mechanical characterization of a pre-fabricated connection system for cross laminated timber structures in seismic regions." *Eng. Struct.* 167 (Jul): 705–715. https://doi.org/10.1016/j.engstruct.2017.12.022.

Popovski, M., and I. Gavric. 2016. "Performance of a 2-story CLT house subjected to lateral loads." *J. Struct. Eng.* 142 (4): E4015006. https://doi.org/10.1061/(ASCE)ST.1943-541X.0001315.

Popovski, M., J. Schneider, and M. Schweinsteiger. 2010. "Lateral load resistance of cross-laminated wood panels." In *Proc., World Conf. on Timber Engineering*, 20–24. Constanta, Romania: Trees and Timber Institute, National Research Council.

Pozza, L., B. Ferracuti, M. Massari, and M. Savoia. 2018. "Axial–shear interaction on CLT hold-down connections–Experimental investigation." *Eng. Struct.* 160 (Apr): 95–110. https://doi.org/10.1016/j.engstruct.2018.01.021.

Priestley, M. N., S. Sritharan, J. R. Conley, and S. Pampanin. 1999. "Preliminary results and conclusions from the PRESSS five-story precast concrete test building." *PCI J.* 44 (6): 42–67. https://doi.org/10.15554/pcij.11011999.42.67.

Sarti, F., A. Palermo, and S. Pampanin. 2016. "Quasi-static cyclic testing of two-thirds scale unbonded posttensioned rocking dissipative timber walls." *J. Struct. Eng.* 142 (4): E4015005. https://doi.org/10.1061/(ASCE)ST.1943-541X.0001291000160.

Sarti, F., T. Smith, A. Palermo, S. Pampanin, and D. Carradine. 2013. "Experimental and analytical study of replaceable buckling-restrained fuse-type (BRF) mild steel dissipaters." In *Proc., New Zealand Society for Earthquake Engineering Annual Conf.* Christchurch, New Zealand: New Zealand Society for Earthquake Engineering.

Smith, T., F. Ludwig, S. Pampanin, M. Fragiacomo, A. Buchanan, B. Deam, and A. Palermo. 2007. "Seismic response of hybrid-LVL coupled walls under quasi-static and pseudo-dynamic testing." In *Proc., 2007 New Zealand Society for Earthquake Engineering Conf., Palmerston North, New Zealand*. Christchurch, New Zealand: New Zealand Society for Earthquake Engineering.

Tatar, A., and D. M. Dowden. 2022. "Analytical and numerical investigation of a low-damage uplift friction damper for self-centering cross-laminated timber rocking walls." *Eng. Struct.* 254 (Mar): 113836. https://doi.org/10.1016/j.engstruct.2021.113836.

Trutalli, D., L. Marchi, R. Scotta, and L. Pozza. 2019. "Capacity design of traditional and innovative ductile connections for earthquake-resistant CLT structures." *Bull. Earthquake Eng.* 17 (Apr): 2115–2136. https://doi.org/10.1007/s10518-018-00536-6.

van de Lindt, J. W., M. O. Amini, D. Rammer, P. Line, S. Pei, and M. Popov. 2020. "Seismic performance factors for cross-laminated timber shear wall systems in the United States." *J. Struct. Eng.* 146 (9): 04020172. https://doi.org/10.1061/(ASCE)ST.1943-541X.0002718.

van de Lindt, J. W., J. Furley, M. O. Amini, S. Pei, G. Tamagnone, A. R. Barbosa, D. Rammer, P. Line, M. Fragiacomo, and M. Popovski. 2019. "Experimental seismic behavior of a two-story CLT platform building." *Eng. Struct.* 183 (Mar): 408–422. https://doi.org/10.1016/j.engstruct.2018.12.079.

Wichman, S. 2023. "Seismic behavior of tall rocking mass timber walls." Ph.D. thesis, Dept. of Civil and Environmental Engineering, Univ. of Washington.

Wichman, S., J. Berman, R. Zimmerman, and S. Pei. 2022b. "Lateral design of a 10-story building specimen with mass timber rocking walls." In *Proc., 12th National Conf. on Earthquake Engineer, 12NCEE*. Oakland, CA: Earthquake Engineering Research Institute.

Wichman, S., J. W. Berman, and S. Pei. 2022a. "Experimental investigation and numerical modeling of rocking cross laminated timber walls on a flexible foundation." *Earthquake Eng. Struct. Dyn.* 51 (7): 1697–1717. https://doi.org/10.1002/eqe.3634.